A TRIDENT SCHOLAR PROJECT REPORT

NO. 447

Uncalibrated Three-Dimensional Microrobot Control

by

Midshipman 1/C James Forrest Cooke, USN

UNITED STATES NAVAL ACADEMY
ANNAPOLIS, MARYLAND

USNA-1531-2

U.S.N.A. --- Trident Scholar project report; no. 447 (2016)

UNCALIBRATED THREE-DIMENSIONAL MICROROBOT CONTROL

by

Midshipman 1/C James Forrest Cooke
United States Naval Academy
Annapolis, Maryland

Certification of Adviser(s) Approval

Professor Samara L. Firebaugh
Electrical and Computer Engineering Department

Professor Jenelle A. Piepmeier
Weapons and Systems Engineering Department

Assistant Professor Hatem ElBidweihy
Electrical and Computer Engineering Department

Acceptance for the Trident Scholar Committee

Professor Maria J. Schroeder
Associate Director of Midshipman Research

USNA-1531-2

REPORT DOCUMENTATION PAGE

Form Approved
OMB No. 0704-0188

1. REPORT DATE *(DD-MM-YYYY)*	**2. REPORT TYPE**	**3. DATES COVERED** *(From - To)*
05-11-2016		

4. TITLE AND SUBTITLE
Uncalibrated Three-Dimensional Microrobot Control

5a. CONTRACT NUMBER

5b. GRANT NUMBER

5c. PROGRAM ELEMENT NUMBER

6. AUTHOR(S)
Cooke, James Forrest

5d. PROJECT NUMBER

5e. TASK NUMBER

5f. WORK UNIT NUMBER

7. PERFORMING ORGANIZATION NAME(S) AND ADDRESS(ES)

8. PERFORMING ORGANIZATION REPORT NUMBER

9. SPONSORING / MONITORING AGENCY NAME(S) AND ADDRESS(ES)
U.S. Naval Academy
Annapolis, MD 21402

10. SPONSOR/MONITOR'S ACRONYM(S)

11. SPONSOR/MONITOR'S REPORT NUMBER(S)
Trident Scholar Report no. 447 (2016)

12. DISTRIBUTION / AVAILABILITY STATEMENT

This document has been approved for public release; its distribution is UNLIMITED.

13. SUPPLEMENTARY NOTES

14. ABSTRACT

The emerging field of microrobotics facilitates precise manipulation of objects at the microscale, which has many applications in medicine and microassembly. This project advanced both sensing and motion capabilities of the Naval Academy's microrobot system, bringing it from a planar system to a three-dimensional system that utilizes an adaptive controller for autonomous operation. Reproducible, robust robot control is particularly challenging at the microscale, where lesser understood surface forces like friction dominate volumetric forces. In such an environment, an adaptive (or "uncalibrated") controller which can dynamically adjust to changes in the operation environment is essential. While many groups have already demonstrated the ability to control a microrobot in three dimensions through magnetically based actuation methods, very few have attempted to apply uncalibrated control algorithms to these systems. This project focused on first developing a magnetic actuation and visual sensor system for a microrobot in a three-dimensional fluidic environment, and then on the development of an uncalibrated controller, utilizing a Recursive Least Squares (RLS) estimation algorithm. With a given desired position, the adaptive controller drives the microrobot to the target position without any prior knowledge of the system parameters such as electromagnetic field strengths, drag coefficients, or intrinsic and extrinsic camera parameters.

15. SUBJECT TERMS
Biomedical Microelectromechanical Systems, Robot Control, Electromagnetics, Visual Servoing, Adaptive Control

16. SECURITY CLASSIFICATION OF:			**17. LIMITATION OF ABSTRACT**	**18. NUMBER OF PAGES**	**19a. NAME OF RESPONSIBLE PERSON**
a. REPORT	**b. ABSTRACT**	**c. THIS PAGE**		26	**19b. TELEPHONE NUMBER** *(include area code)*

ABSTRACT

The emerging field of microrobotics facilitates precise manipulation of objects at the microscale, which has many applications in medicine and microassembly. This project advanced both sensing and motion capabilities of the Naval Academy's microrobot system, bringing it from a planar system to a three-dimensional system that utilizes an adaptive controller for autonomous operation. Reproducible, robust robot control is particularly challenging at the microscale, where lesser understood surface forces like friction dominate volumetric forces. In such an environment, an adaptive (or "uncalibrated") controller which can dynamically adjust to changes in the operation environment is essential. While many groups have already demonstrated the ability to control a microrobot in three dimensions through magnetically based actuation methods, very few have attempted to apply uncalibrated control algorithms to these systems. This project focused on first developing a magnetic actuation and visual sensor system for a microrobot in a three-dimensional fluidic environment, and then on the development of an uncalibrated controller, utilizing a Recursive Least Squares (RLS) estimation algorithm. With a given desired position, the adaptive controller drives the microrobot to the target position without any prior knowledge of the system parameters such as electromagnetic field strengths, drag coefficients, or intrinsic and extrinsic camera parameters.

Keywords: Biomedical Microelectromechanical Systems, Robot Control, Electromagnetics, Visual Servoing, Adaptive Control

ACKNOWLEDGEMENTS

Working on this Trident project was a great experience for my senior year. The opportunities and challenges this program presented me are invaluable in my development as an officer in the United States Navy. While I worked tirelessly on this project, I could not have completed the project without the help and advice of many people throughout the yard.

First, I would like to thank my three advisors: Professor Samara Firebaugh, Professor Jenelle Piepmeier, and Professor Hatem ElBidweihy. Without their guidance for the last year and a half, this project would not have been possible. They have shaped and guided my efforts into a successful academic venture that I am proud to have taken part in.

Next, I would like to thank Mr. Marcus Sydnor of the Electrical and Computer Engineering Laboratory, Mrs. Louise Becnel of the Fluids Laboratory, Mr. Joe Bradshaw, Mr. Nick Eagle, Mrs. Nan Nawrocki, and Mr. Norm Tyson of the Weapons and Systems Engineering Laboratory, and Mr. Mike Superczynski of the Project Support Branch for their assistance tackling many of the technical and material challenges I throughout the project. Also, Professor Charles Nelson was very generous to loan us fixturing hardware during the construction of the system.

I would also like to thank CAPT Owen Thorp and CDR Kevin Doney for their support in my selection as a Trident Scholar.

Finally, I would like to thank my roommates, MIDN 1/C Dean Corbett and MIDN 1/C Mathew Miller, for entertaining my late-night study habits while working on this project, and my parents, Mike and Karen Cooke, for helping me revise my application and reports numerous times.

Without all these people, this project would not have been possible.

TABLE OF CONTENTS

I. INTRODUCTION

Microrobotic systems refer to robotic systems for which the end effector is tetherless and on the micrometer to millimeter scale (10^{-6} to 10^{-3} m). They have a wide range of emerging medical, biological, and industrial applications. Two of the most promising areas this technology can affect are bio-manufacturing and medical procedures. Some of the technical challenges that face microrobotics include the difficulty of transferring power and control signals to the microrobot and the dominance of surface forces such as friction over volumetric forces on microrobot motion. This is of particular difficulty for operation within a widely varying biological environment.

This project focused on the development of an uncalibrated three-dimensional controller for magnetically actuated microrobots in fluidic environments. While "uncalibrated" often is used in a negative connotation in other engineering disciplines, in the field of microrobotics, "uncalibrated" is a desirable system characteristic equivalent to "adaptive or "self-calibrating." The system operates without any prior knowledge of the exact electromagnet geometry, drag coefficients, magnetic field strengths, camera parameters, microrobot structure, and fluidic operating environment. Furthermore, the controller can adapt to changes that might occur during operation. Because biological systems are complex and dynamic, uncalibrated controllers are ideal for microrobot applications in medical operations.

This project expands on previous research in microrobotics conducted by midshipmen at USNA. At the start of this project, the Naval Academy had a microrobot system based on magnetic actuation that utilized an uncalibrated control method for two-dimensional motion. In this system, the microrobot was a ferromagnetic piece of material, suspended at a fluid interface (between oil and saline) to confine its motion to two dimensions. The controller was adaptive and based on a Recursive Least Square (RLS) Jacobian estimation algorithm [1]. Figure 1 depicts the original system.

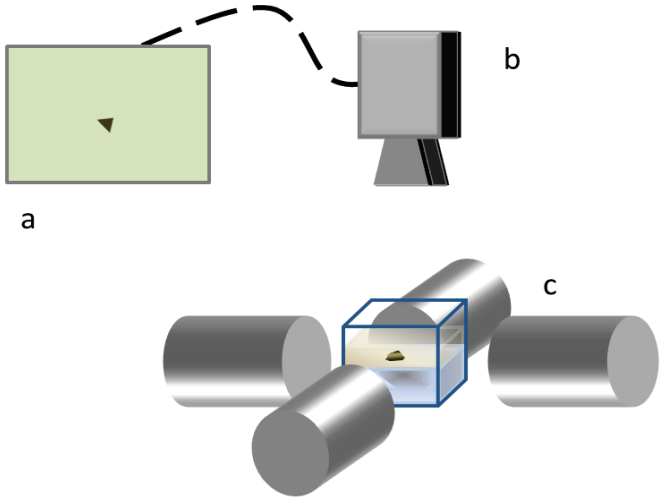

Figure 1. The Naval Academy's 2-D magnetic actuated microrobot control system. The microrobot is observed on a computer screen (a) in an image that is captured from a camera attached to a microscope (b). The microrobot itself lies at a fluid interface and is actuated with the use of four electromagnets (c). [1]

This project extended the existing system to accommodate three-dimensional controlled motion. This required expanding the system's three-dimensional vision capabilities, implementing a system capable of three-dimensional actuation, and creating a LabVIEW program able to manage three-dimensional control.

II. THEORY

While the control strategy employed does not require a model of the microrobot system, an understanding of the underlying physics can inform the design choices for the system. This section describes the forces experienced by the microrobot and develop the relationship between magnetic forces and translational motion. This relationship provides insight into the applicability of the Recursive Least Squares Jacobian Estimation method as an adaptive controller.

A. Magnetic Actuation

The forces acting on the microrobot include gravitational forces, drag forces, buoyancy forces, and magnetic forces. Figure 2 depicts body forces acting on a microrobot along with the coordinate system. Let $\vec{r}_w$ represent the position of the microrobot, $[x\ y\ z]_w{}^T$ with respect to a fixed world coordinate frame [2]. The equation of motion for the microrobot is given by:

$$\vec{F}_m + \vec{F}_d + \vec{F}_g + \vec{F}_b = m\ddot{\vec{r}}_w \tag{1}$$

In Equation 1, $\vec{F}_m$ is the applied magnetic force, $\vec{F}_d$ is the hydrodynamic drag force from the fluid on the microrobot, $\vec{F}_g$ is the force from gravity, $\vec{F}_b$ is the buoyancy force, and $m\ddot{\vec{r}}_w$ represents the mass of the microrobot times the its acceleration in the direction w [3]. $\vec{F}_m$, $\vec{F}_d$, and $m\ddot{\vec{r}}_w$ act in all three dimensions, while $\vec{F}_g$ and $\vec{F}_b$ act only in the z direction.

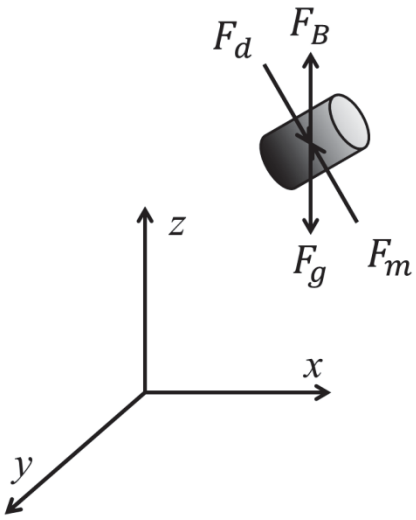

Figure 2. Forces acting on the microrobot in low Re number flow along with the global coordinate system [3].

The microrobots used in this system are composed of soft ferromagnetic materials. For the microrobot to experience translational force there must be a spatial variation in the magnetic field as illustrated in Figure 3.

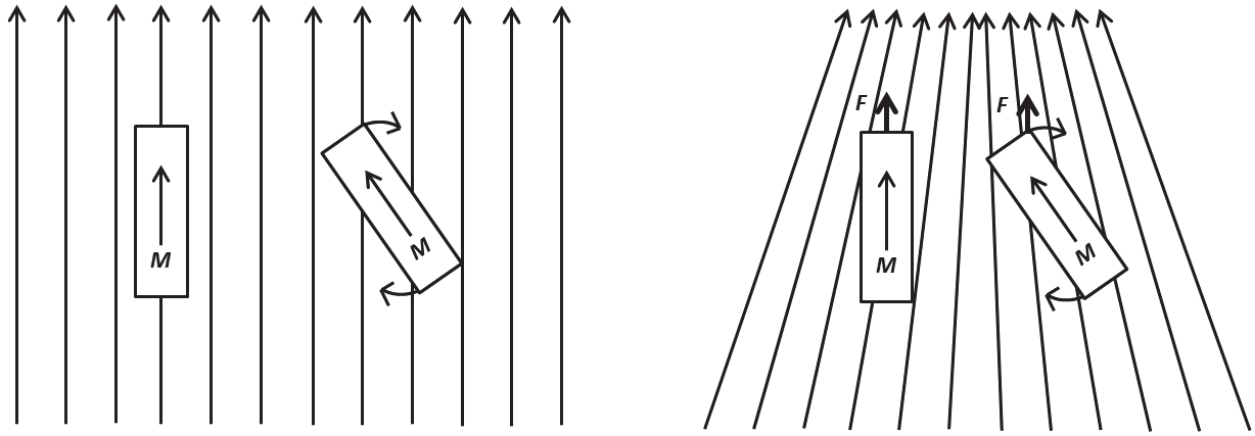

Figure 3. The left diagram shows a uniform magnetic field creating a torque which could be used to control the orientation of the object. Attitude control of a microrobot is not one of this project's goals. The right diagram shows a non-uniform field developing both a torque and a net translational force on the ferromagnetic object due to the gradient of the field. This project will utilize case B. because the goal of the project is to control a microrobot's position using forces from a magnetic field.

The equation for magnetic force is given by:

$$\vec{F}_m = \left(\vec{M} \cdot \vec{\nabla}\right)\vec{B}\left(\vec{P}\right) \tag{2}$$

In this equation, the magnetic force $\vec{F}_m$ on the microrobot is a function of the magnetic moment $\vec{M}$, applied magnetic flux density $\vec{B}$, and microrobot position $\vec{P}$. For ferromagnetic materials, the magnetic moment is related to the magnetic flux density [4].

The magnetic force depends on both the absolute magnetic flux and on the gradient of the magnetic flux. Equation 2 can be rewritten into matrix form as:

$$\begin{bmatrix} F_{m_x} \\ F_{m_y} \\ F_{m_z} \end{bmatrix} = \begin{bmatrix} \frac{\partial B_x}{\partial x} & \frac{\partial B_y}{\partial x} & \frac{\partial B_z}{\partial x} \\ \frac{\partial B_x}{\partial y} & \frac{\partial B_y}{\partial y} & \frac{\partial B_z}{\partial y} \\ \frac{\partial B_x}{\partial z} & \frac{\partial B_y}{\partial z} & \frac{\partial B_z}{\partial z} \end{bmatrix} \begin{bmatrix} M_x \\ M_y \\ M_z \end{bmatrix} = \begin{bmatrix} M_x \left\| \vec{\nabla} B_x \right\| \\ M_y \left\| \vec{\nabla} B_y \right\| \\ M_z \left\| \vec{\nabla} B_z \right\| \end{bmatrix} \tag{3}$$

The drag forces acting on the microrobot can be linearized according to Stoke's Flow when assuming a spherical shape [5]; however, exact modeling of the drag forces is unneeded due to the uncalibrated nature of the system. Linearizing the drag coefficients (α, β, γ), as seen in [2] and inserting Equation 3 into the results in the linearized equation of motion:

$$m \begin{bmatrix} \ddot{x} \\ \ddot{y} \\ \ddot{z} \end{bmatrix}_w = \begin{bmatrix} \alpha & 0 & 0 \\ 0 & \beta & 0 \\ 0 & 0 & \gamma \end{bmatrix} \begin{bmatrix} \dot{x} \\ \dot{y} \\ \dot{z} \end{bmatrix}_w + \begin{bmatrix} 0 \\ 0 \\ \vec{F}_g + \vec{F}_b \end{bmatrix} + \begin{bmatrix} M_x \left\| \vec{\nabla} B_x \right\| \\ M_y \left\| \vec{\nabla} B_y \right\| \\ M_z \left\| \vec{\nabla} B_z \right\| \end{bmatrix} \tag{4}$$

In previous Naval Academy microrobot work, it was assumed that the buoyant forces cancelled the gravitational forces, because the microrobot was acting at an interface between two fluids of different densities. This assumption cannot be made for all microrobots acting in a three-dimensional fluid volume, because the object will not be acting at an interface, but instead will be completely submerged in a single fluid. Depending on the fluid and the microrobot design, this assumption may no longer be true if buoyancy and gravitational forces are no longer of the same order of magnitude.

Equation 4 can be further simplified, because microrobots act at low Reynolds numbers, meaning that the inertial force on the left side of Equation 4 is much less than the body forces on the right side of the equation [2]. Thus, the inertial forces can be considered negligible, and Equation 4 can be reduced to:

$$0 \cong \begin{bmatrix} \alpha & 0 & 0 \\ 0 & \beta & 0 \\ 0 & 0 & \gamma \end{bmatrix} \begin{bmatrix} \dot{x} \\ \dot{y} \\ \dot{z} \end{bmatrix}_w + \begin{bmatrix} 0 \\ 0 \\ \vec{F}_g + \vec{F}_b \end{bmatrix} + \begin{bmatrix} M_x \left\| \vec{\nabla} B_x \right\| \\ M_y \left\| \vec{\nabla} B_y \right\| \\ M_z \left\| \vec{\nabla} B_z \right\| \end{bmatrix} \tag{5}$$

The magnetic gradient produced by a coil is linearly related to the current passing through the coil (which is generated by a pulse width modulated voltage square wave from the computer).

B. Control Theory

The overall system relationship between the actuation current signal and the microrobot velocity is described by the Jacobian matrix. Equation 6 shows the linear relationship between the actuation current signal, $\vec{u}(t)$, and the microrobot velocity, $\dot{\vec{r}}_p(t)$, where $J(r)$ is Jacobian matrix.

$$\dot{\vec{r}}_p(t) \cong J(r)\vec{u}(t) \tag{6}$$

The Jacobian matrix reflects the properties of the camera, the drag coefficients, magnetic moments, magnetic field strengths and gradients, system geometry and material properties. This matrix fluctuates as the microrobot moves throughout the arena. While computing a closed form solution for $J(r)$ is possible, doing so requires calibration and consistency in system parameters. Therefore, a system that does not require calibration is more widely applicable and robust.

For the microrobot system, the observed position of the object, $\vec{r}$, will change as a the control signal from Equation 6, $\vec{u} \in \mathbb{R}^n$, is applied to the system. The desired position of the microrobot is denoted by $\vec{r}^*(t)$, and the error, $f \in \mathbb{R}^m$, is the difference between the observed and desired position of the microrobot [2].

$$f\big(r(t)\big) = \vec{r}(t) - \vec{r}^*(t) \tag{7}$$

For a planar, two degrees of freedom, visual control system, $m = 2$ and $n = 2$, because the microrobots position can be measured by a single camera and because there are two opposing pairs of electromagnets in the system, respectively. As the system is expanded to control higher degrees of freedom, such as orientation of the microrobot or three-dimensional control, the values of *m* and *n* will increase.

$$F\big(r(t)\big) = \tfrac{1}{2} f\big(r(t)\big)^T f\big(r(t)\big) \tag{8}$$

The goal of the system is to calculate a control signal that will both minimize the $F(r(t))$ image error squared and drive the microrobot to the desired position, $\vec{r}^*(t)$ [2]. The control signal is computed via a quasi-Newton method operating an iteratively estimated Jacobian as seen in [6] [7] [8]. A special case of the Kalman filter [9], the RLS method presented in [8] will be used for its ability to follow moving targets and superior performance in the occurrence of system noise.

In order to solve for control signal and Jacobian matrix, a discrete control algorithm is updated at iteration k with a digital sampling time h_t. Let r_k represent the microrobot's position in the image plane at the k^{th} iteration, r_k^* denote the target position in the image plane at the k^{th} iteration, Δf_k signify the change in image error $f_k - f_{k-1}$, and u_k characterize the actuation signal for the electromagnets. The RLS estimate for the Jacobian matrix $\hat{J}_k$ is given by Equation 11 below, and the actuation signal is calculated in Equation 13 below. The entire iterative control algorithm is given in the Recursive Least Squares Estimation Algorithm [2].

RLS Algorithm: Given: $f \in \mathbb{R}^m$; $u_0, u_1 \in \mathbb{R}^n$, $\hat{J}_0 \in \mathbb{R}^{m\times n}$, $P_0 \in \mathbb{R}^{n\times n}$, $\lambda \in (0,1)$

Do for $k = 1,2, \ldots$

$$\Delta f_k = f_k - f_{k-1} \tag{9}$$

$$\frac{\partial r_k^*}{\partial t} h_t = r_k^* - r_{k-1}^* \tag{10}$$

$$\hat{J}_k = \hat{J}_{k-1} + \frac{\left(\Delta f_k - \hat{J}_{k-1}u_k + \frac{\partial r_k^*}{\partial t}h_t\right)u_k^T P_{k-1}}{\lambda + u_k^T u_k} \tag{11}$$

$$P_k = \frac{1}{\lambda}\left(P_{k-1} - \frac{P_{k-1}u_k u_k^T P_{k-1}}{\lambda + u_k^T P_{k-1} u_k}\right) \tag{12}$$

$$u_{k+1} = -\left(\hat{J}_k^T \hat{J}_k\right)^{-1} \hat{J}_k^T \left(f_k - \frac{\partial r_k^*}{\partial t} h_t\right) \tag{13}$$

End for

End

Equation 11 estimates the relationship between the actuation signal from the previous iteration and the observed change in error for each iteration k. Equation 13 then uses this new estimation of the Jacobian to calculate a new actuation signal that drives the microrobot towards the desired target. In Equation 12, P_k is the estimated value of the covariance matrix of the actuation signal, and λ is the weighting factor which prevents noise in the term Δf_k from causing erratic estimations of the Jacobian matrix. Values of λ closer to 1 yield longer memory, and values of λ greater than 0.9 often are typical for the algorithm [2] [10]. In Equation 10, the term $\frac{\partial r_k^*}{\partial t} h_t$ represents the target velocity, which is set to zero for a stationary target. Overall, the algorithm results in a control scheme that adaptively learns the correlation between the control actuation signal and the robot velocity and is capable of driving the robot to a desired stationary or moving target even in the presence of noise. The algorithm can control various microrobot device shapes at various optical zoom settings with no system modeling or calibration [2]. This algorithm has already been applied to the Naval Academy's two-dimensional microrobot system, and will work for any system so long as $m \geq n$, buoyancy forces are on the order of gravitational forces, and a reasonable relationship between microrobot motion and imaging noise exists [2].

III. Experimental Method

The proposed uncalibrated controller adaptively learns the relationship between the actuation signal and device's motion. However, such a controller can only succeed with a thoughtfully designed system that is capable of both generating and sensing microrobot motion. Before applying the controller, significant modifications were required to implement three-dimensional visual sensing and actuation. This required systematic modification, testing, and troubleshooting. In the following sections, the development of the vision system, electromagnet array, mechanical fixturing, and control algorithms are detailed.

A. System Vision Modifications

To allow for visual feedback of the microrobot's position in all three dimensions, a second camera was added to the system. This is illustrated in Figure 4. The second camera views the operating arena from the side at a varying focal length based upon the zoom of the lens attached to the camera. With a 1.0x lens adapter tube and a Navitar 12X Zoom lens, the working distance of the side camera was roughly 15cm. For most of our data, the top camera used a working distance of 10cm at a magnification of 4.5X. With these settings, the pixel size in both views is approximately the same with one pixel approximately equal to about 20 micrometers. The two camera system allowed for tracking of the microrobot in all three-dimensions. One camera viewed the operating area from the top and tracked the x-y position of the microrobot relative to the image frame. The second camera viewed the operating area from the side and tracked the z position relative to that camera's image coordinate frame. These two cameras are connected to the computer. To integrate the cameras with LabVIEW, code was written to display both cameras' feeds in real time.

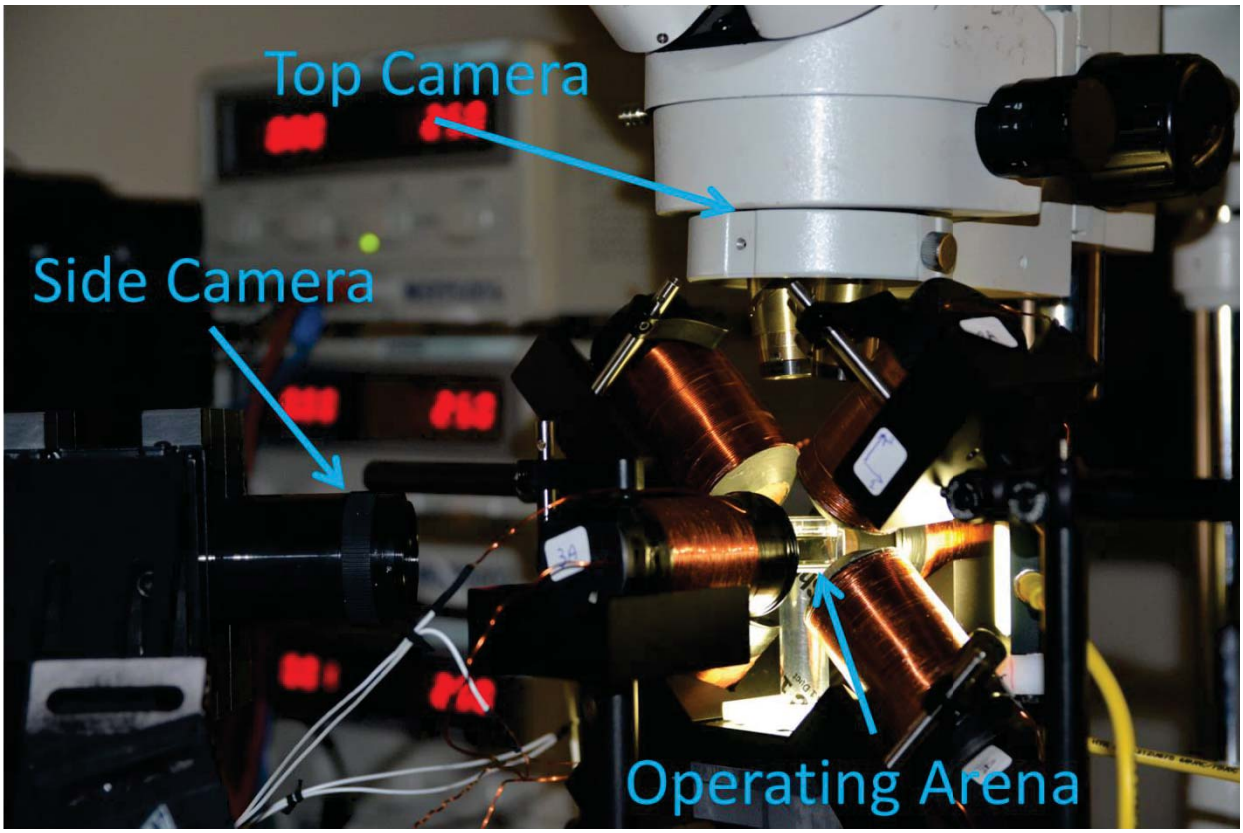

Figure 4. The final microrobot system.

One concern with the vision system was that as the microrobots moved about the workspace, they would move out of the focal plane of the cameras and become too blurry for the computer to accurately sense position. However, in our experiments we found that the vision system gave us a working volume of about $3mm \times 3mm \times 3mm$, which was sufficient for the demonstration of three-dimensional controlled motion.

Numerous coding changes were made to the vision thresholding system. The camera feeds were sent to the PC via USB cable. Since the microrobot is silhouetted by backlighting, the raw picture was thresholded into a binary image to select dark pixels. Particulates and lighting variations can result in false positives. The previously-existing code simply selected the first object in this binary image. This method proved problematic for the three-dimensional system, as the false positives in the camera feeds were making it difficult for the computer to accurately locate the microrobot. Changes made to the code allowed for the selecting of a rectangular area to exclude structural features that distorted the binary image data.

The code then went through the smaller rectangular area to find objects within a user selected object area range. This method allowed for accurate isolation of the microrobot in the image so that the control could perform optimally and not lose the position of the microrobot. The process for thresholding the vision data is shown in Figure 5.

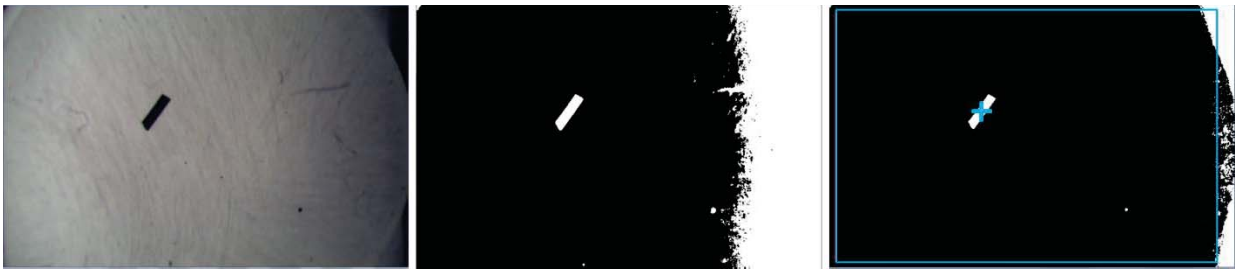

Figure 5. Process for thresholding position of microrobot with the top camera. The left image shows the camera output. The middle image shows the binary transform with a threshold limit of 100. The right image shows the binary transform with a threshold limit of 70 and a blue rectangle displaying the search area and a blue cross marking the center of the selected object. The same process is executed for the side camera.

B. System Actuation Modifications

In order to operate in three dimensions, the electromagnet setup was modified to supply higher magnetic forces and gradients to the microrobot. In particular, the original radial electromagnets were replaced with axial electromagnets. Both types of electromagnets provide the non-uniform magnetic fields needed to actuate the microrobot's motion. But, while axial electromagnets produce strong magnetic fields and weaker gradients, radial electromagnets produce fields with stronger gradients but weaker field magnitudes. The force experienced by the robot, as described in the theory section above, depends on both the field gradient and on the absolute value of the field (which affects the magnetization of the robot). To determine the best electromagnets for the system, four different axial electromagnets that varied in power draw, output average flux density, and size [11] were tested. Using a Gaussmeter, the field for each electromagnet was mapped for different voltage levels, as is shown in Figure 6. A similar study was done in [12]. These measurements allowed us to examine the effects that different electromagnets had on the actuation of the microrobot. The final system utilized six axial electromagnets.

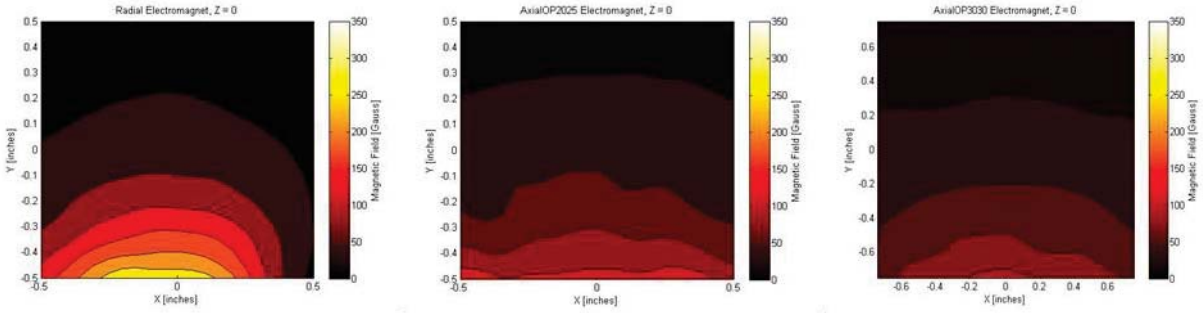

Figure 6. The magnetic field in Gausses produced from varying types of electromagnets. The left graph shows the magnetic field produced by a radial electromagnet. The middle graph shows the magnetic field produced by a two inch diameter axial electromagnet. The right graph shows the magnetic field produced by a three inch diameter axial electromagnet.

As discussed in section II.A., microrobot motion is produced in the presence of a magnetic gradient, and the steepness of that gradient will affect the magnitude of microrobot's velocity. Thus, it follows that by varying the average voltage applied to the electromagnet, the speed can be controlled. To do this, a technique used commonly in controlling motors known as Pulse Width Modulation (PWM) is utilized. A high frequency square wave is applied across the electromagnetic leads. The frequency of the signal is faster than the time constant of the electromagnet, and the system responds solely to the average applied voltage. By varying the duty cycle of the square wave, the average voltage is increased or decreased. Control signals thus range from a 0% duty cycle (0V) to a 100% duty cycle (25V).

While pulse-width modulation was also employed with the 2D system, further changes to the two-dimensional system were required to accommodate the added electromagnets. The power output of the computer's data acquisition unit is small, so driver circuitry was required to provide the electrical current necessary for the electromagnets. The circuit for driving a single electromagnet is shown in Figure 7 below. This is a simple MOSFET switching circuit with a flyback diode which prevents the voltage spike that normally would occur when switching the current flowing through the electromagnet's large inductance. This circuit was replicated six times for the three-dimensional driver. Circuits for opposite electromagnets were paired together with separate power sources so that the circuits were labeled 1A, 1B, 2A, 2B, 3A, and 3B. This pairing was done to reduce the chances of overloading the power source. Below, Figure 8 compares the two-dimensional driver circuitry box to the three-dimensional driver circuitry box. As part of this effort the screw plate wire connectors were also replaced with user-friendly quick disconnect connectors.

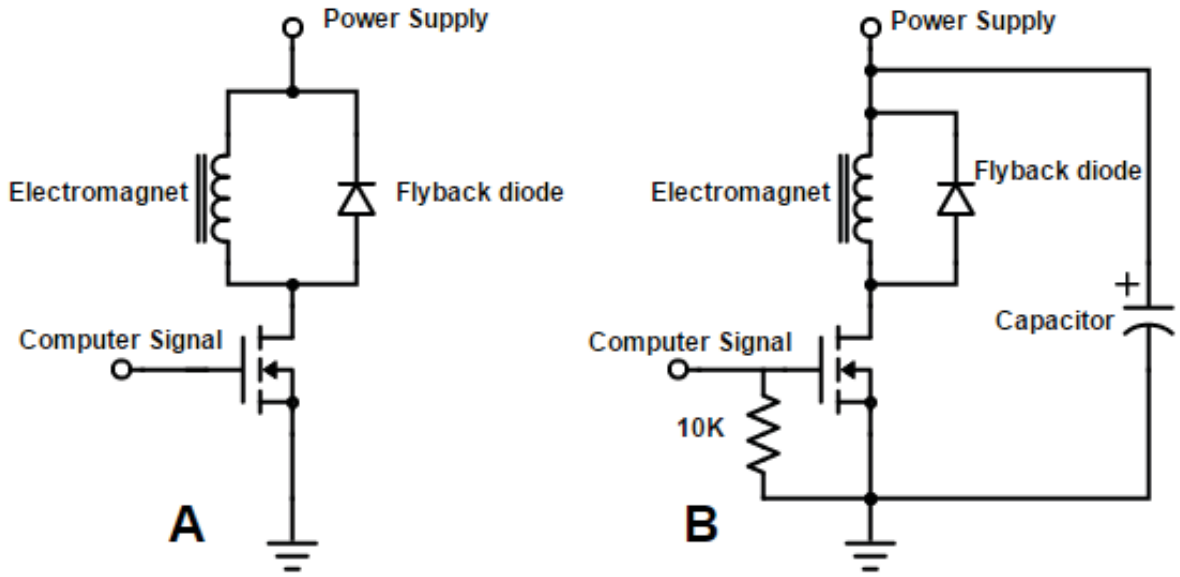

Figure 7. The driver circuit or an electromagnet. Circuit A was used on the two dimensional microrobot control system. Circuit B was implemented into the three-dimensional microrobot control system. A 10kΩ pull-down resistor and a capacitor were added to the circuit to prevent shorting the circuit.

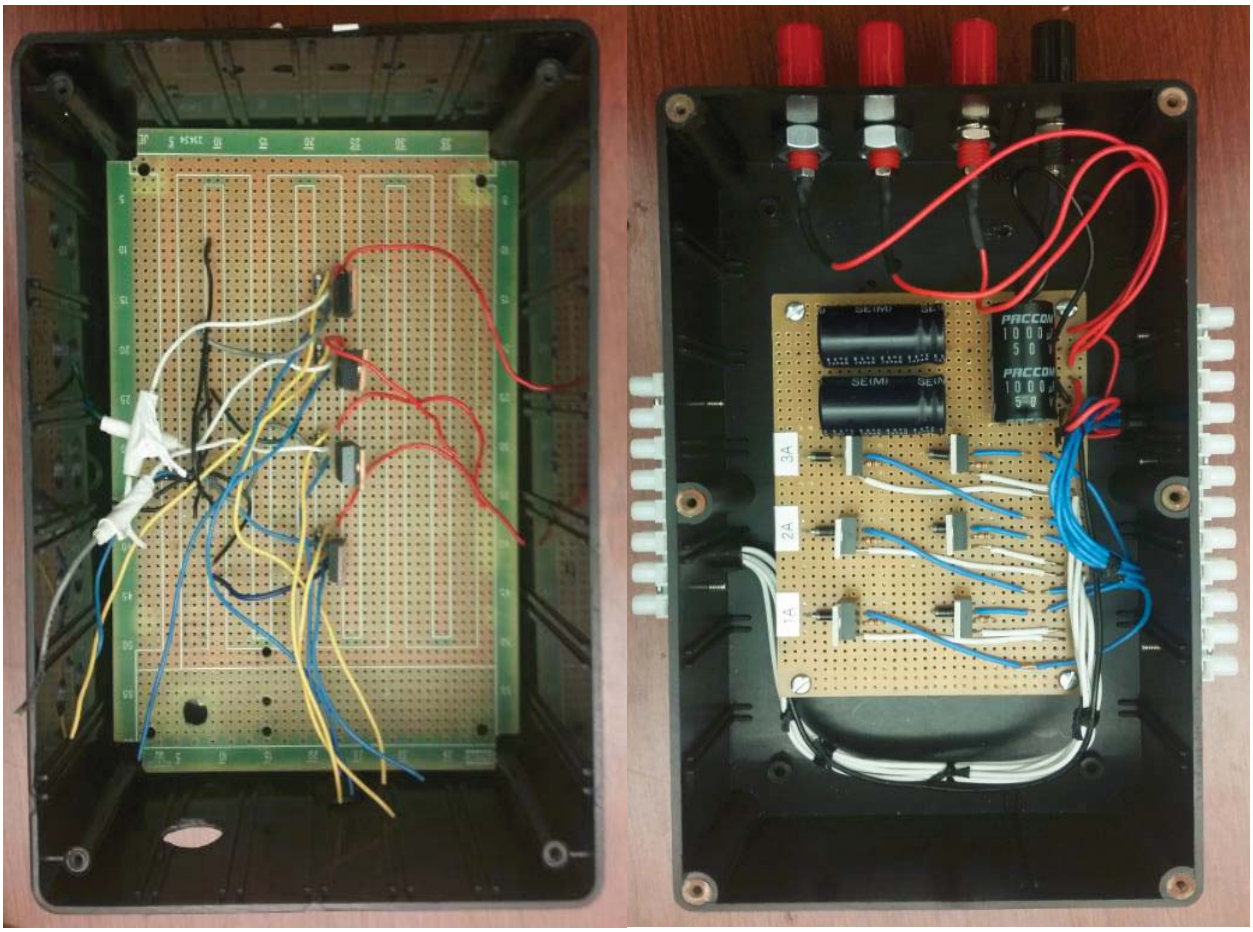

Figure 8. The driver box for the electromagnets. The board on the left was used in the two dimensional microrobot control system. The board on the right is used in the three-dimensional microrobot control system. The quick disconnect connections can be seen along the edges of the image on the right.

C. System Fixture Modifications

Once the type of electromagnet was selected, a selection of optical fixtures were purchased to allow for reconfigurable positioning of all the components of the system—the six electromagnets, two cameras with magnifying lenses, backlights for each camera, and the fluid cell in which the microrobot operated. Numerous constraints limited the design of the final system. First, the two cameras needed to be able to collectively view the *x*-*y*-*z* movement of the microrobot, and backlights needed to be placed opposite of these cameras and behind the operating arena. These two constraints limited how close the electromagnets could be placed to the operating arena where the microrobot interacted. Conversely, the electromagnets needed to be placed close to the operating arena in order to provide a large of a magnetic field to control the microrobot. Next, the electromagnets needed to be configured orthogonally to match the design of our control system. Figure 4 shows the complete system, which allows for precise positioning of the different system components. A new fixture was created to hold the vial containing the liquid and the microrobot. The fixture, seen in Figure 9, made it possible to place magnets beneath the vial without blocking the light from the backlight from reaching the operating arena.

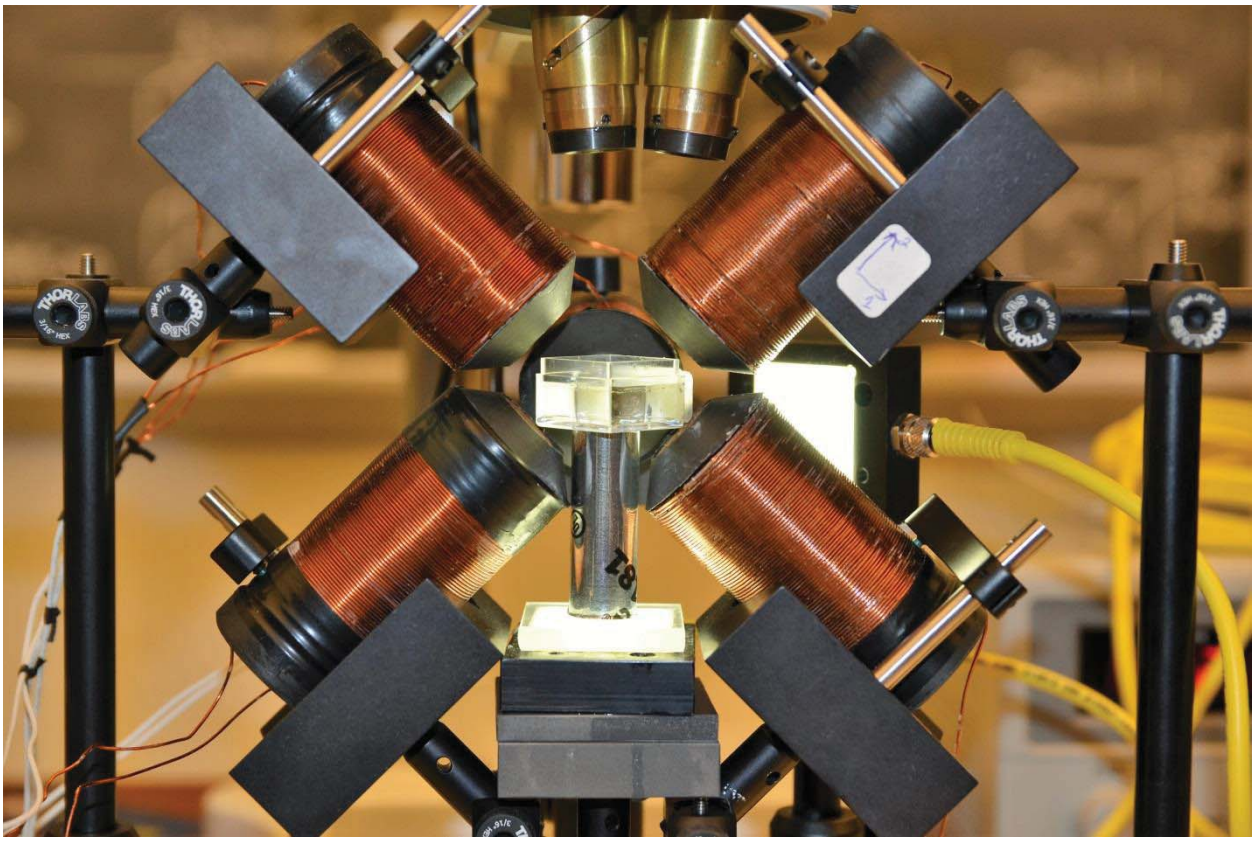

Figure 9. The narrow, cylindrical stand that allows for close placement of electromagnets near the vial containing the microrobot. The stand consists of clear acrylic wrapped in reflective tape to allow the backlighting to be transmitted through the stand.

Implemented into the controller is a coordinate shift that alters the *x*-*y*-*z* axes into the 1-2-3 axes displayed in Figure 10. This coordinate shift aligns the electromagnet pairs to the desired direction of control. To implement this shift, the position of the microrobot in *x*-*y*-*z* coordinates is sent through Equation 14, shown below.

$$\begin{bmatrix} r_1 \\ r_2 \\ r_3 \end{bmatrix} = \begin{bmatrix} \cos 45° & 0 & -\sin 45° \\ \sin 45° & 0 & \cos 45° \\ 0 & -1 & 0 \end{bmatrix} \begin{bmatrix} r_x \\ r_y \\ r_z \end{bmatrix} \tag{14}$$

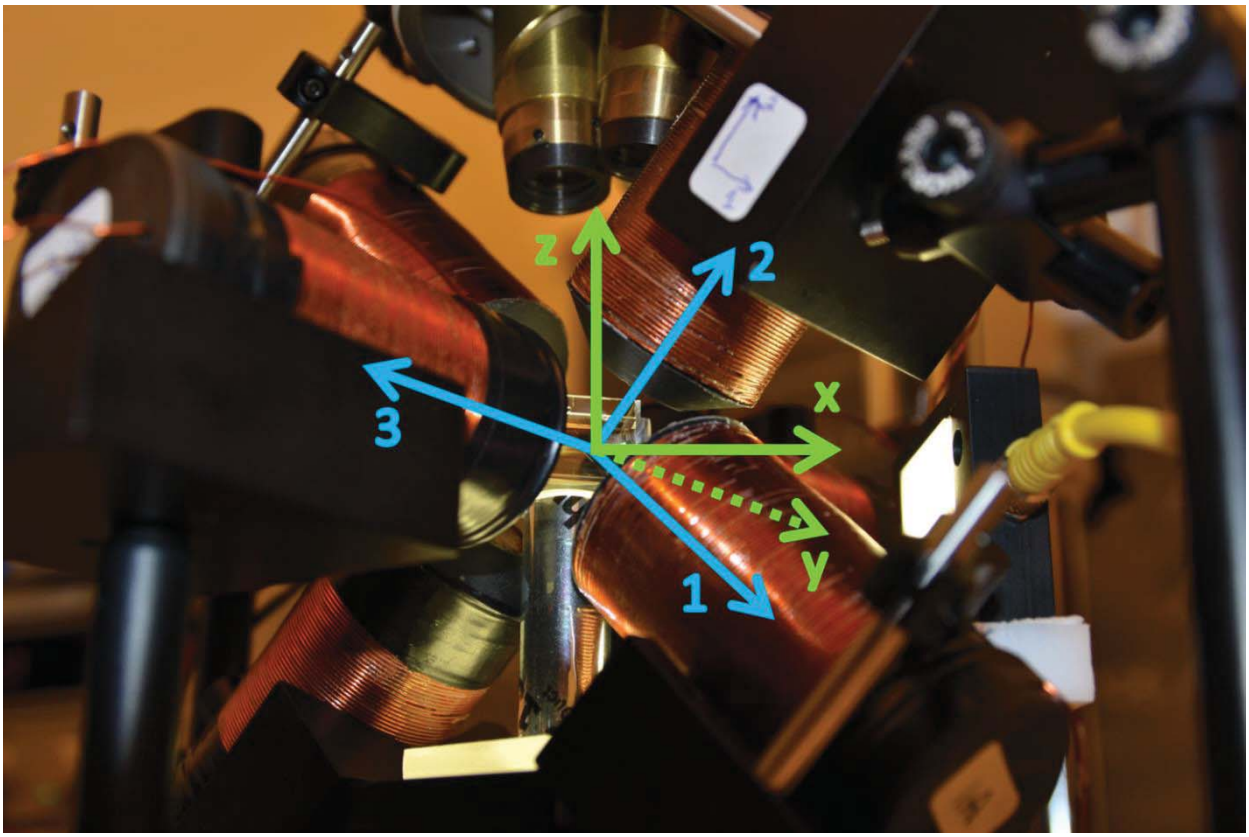

Figure 10. The coordinate transform for the control system to align the electromagnet pairs with the desired direction of control.

D. Controller Development

The LabVIEW code implements multiple control methods to achieve teleoperation in three dimensions. The first method required a user to select which direction he or she wanted the microrobot to move using input from the keyboard of the PC. This step demonstrates basic control of the microrobot in three dimensions. This control method was crucial in determining what combination of microrobot, fluid, voltage, and duty cycle could accomplish control in the x, y, and z directions. This control method was also utilized as a means of placing the microrobot in the observable region of the cameras. The open loop control is described in Algorithm 1.

Algorithm 1: Open-loop Control

$Do\ for\ k = 1,2, \ldots$

$User\ observes\ position\ of\ microrobot\ in\ camera\ display$

$User\ decides\ which\ electromagnet\ to\ activate\ and\ presses\ down\ one\ of\ six\ keys$

$Computer\ reads\ which\ key\ was\ pressed\ down\ by\ user$

$PWM\ signal\ sent\ to\ selected\ electromagnet$

$Selected\ electromagnet\ activates\ and\ creates\ magnetic\ field$

$Microrobot\ moves$

$End\ for$

End

The second method employed a proportional controller. Classically, a proportional controller computes the control signal by multiplying the error by a constant gain and is the simplest of feedback control methods. This program demonstrated the system's ability to sense the position of the microrobot, decide what direction the microrobot needed to move, and actuate the correct series of electromagnets to accomplish the user's goal. This program helped to debug the control actuation method and to map which electromagnet needed to be actuated in order to lessen the error between the misticrorobot's desired and actual position. The gain matrix must be provided by the user and requires *a priori* observation. The proportional controller is described in Algorithm 2.

Algorithm 2: Proportional Control

$Do\ for\ k = 1,2, \ldots$
$Locate\ microrobot\ position\ in\ images\ using\ machine\ vision$
$Transform\ microrobot\ position\ from\ xyz\ to\ electromagnet\ coordinate\ frame$
$Compute\ error\ between\ desired\ and\ actual\ microrobot\ position\ in\ pixels$
$Duty\ cycle = gain * error$
$PWM\ signal\ sent\ to\ selected\ electromagnets$
$Selected\ electromagnets\ activate\ and\ create\ magnetic\ field$
$Microrobot\ moves$
$End\ for$
End

The third method utilized the Recursive-Least-Squares algorithm to accomplish truly uncalibrated control of the microrobot, which is described in Algorithm 3.

Algorithm 3: Uncalibrated Control

$Do\ for\ k = 1,2, \ldots$
$Locate\ microrobot\ position\ in\ images\ using\ machine\ vision$
$Transform\ microrobot\ position\ from\ xyz\ to\ electromagnet\ coordinate\ frame$
$Compute\ error\ between\ desired\ and\ actual\ microrobot\ position\ in\ pixels$
$Update\ Jacobian\ matrix$
$Update\ P\ (Covariance) matrix$
$Duty\ Cycle = (inverse\ of\ Jacobian) * error$
$PWM\ signal\ sent\ to\ selected\ electromagnets$
$Selected\ electromagnets\ activate\ and\ create\ magnetic\ field$
$Microrobot\ moves$
$End\ for$
End

There were multiple challenges with implementing the uncalibrated control. The first obstacle came with deciding where to apply the coordinate transform in the uncalibrated control. Originally, the transformation executed just before the duty cycles were calculated. This methodology caused problems for the RLS algorithm because the algorithm was calculating the updated Jacobian and covariance matrix based off the *x*-*y*-*z* error rather than the transformed 1-2-3 axes error. For the system to work, the coordinate transform had to be placed immediately after the microrobot was located by the vision thresholding system.

Combatting the effects of gravity and high surface forces provided another obstacle for the uncalibrated control. The controller is developed with some simplifying assumptions that neglect these forces. The high surface attraction forces require a strong magnetic force to lift the microrobot off the bottom of the vial, but once suspended, much smaller forces were necessary for control. Conversely, the gravitational forces on the microrobot constantly worked against the uncalibrated control code's progress in reducing vertical error. This challenge stems from the assumption made in the controller that gravity forces and buoyancy forces cancelled. The solution was found in the use of liquids viscous enough to slow the descent of the microrobot, while not being so thick as to limit the motion of the microrobot entirely. The combination of microrobot and fluid found to work best to overcome these forces was a 1 mm steel rod, with a diameter of approximately 340 microns, placed in a solution of corn syrup.

Even with the combination of steel and corn syrup, the uncalibrated controller sometimes seemed unable to converge on the solution. This problem was eliminated by slowing down the sampling rate of the controller to reduce the effects of noise on the system. At too high of a sample rate, the distance moved in a cycle was on the same order of magnitude as the imaging noise. With the sample rate decreased, stability was achieved with the uncalibrated controller.

IV. RESULTS

To test the uncalibrated controller's effectiveness over a classical control method, the system was tested under a variety of conditions. The nominal condition included the same electromagnet and camera setup as seen in Figure 4, with 25 Volts supplied to each electromagnet, the side camera set to a magnification of 12X, the top camera set to a magnification of 4.5X, and the 1mm steel rod placed in a solution of corn syrup. At this nominal condition, both the results of the uncalibrated and the proportional controller can be seen in Figures 11, 12, and 13.

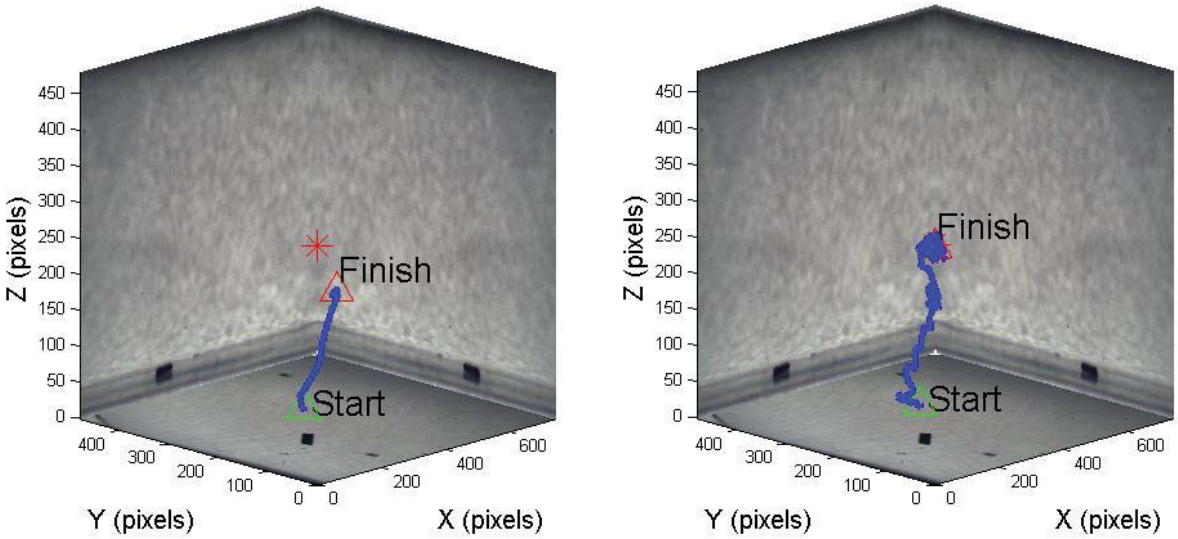

Figure 11. Three-dimensional path of the microrobot at the system's nominal structure. The left graph shows the path in the image space of the proportional controller and the right graph shows the path in the image space of the uncalibrated controller.

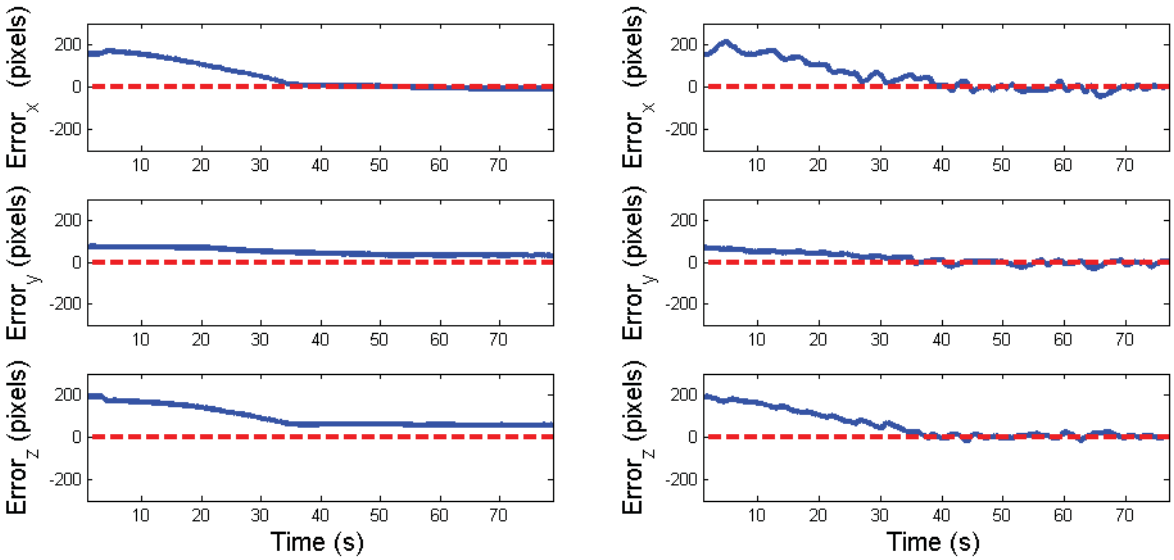

Figure 12. Error between the target and actual microrobot position at the system's nominal structure. The left graph shows the error of the proportional controller and the right graph shows the error of the uncalibrated controller.

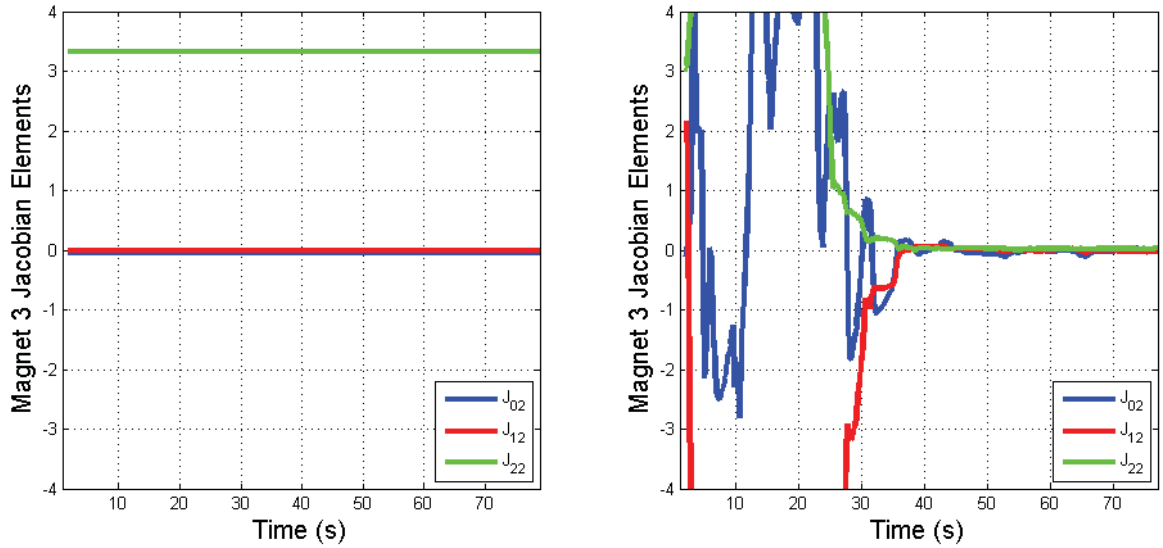

Figure 13. Values of the bottom row of the 3x3 Jacobian matrix at the system's nominal structure. The left graph shows the unchanging "Jacobian" values in the proportional controller and the right graph shows the adapting values of the estimated Jacobian. Note that for the proportional control, the control gains are implemented as a diagonal "Jacobian" matrix with constant values.

As shown by both Figure 11 and 12, the uncalibrated controller was able to drive the position of the microrobot to the target position. The proportional controller was stable but exhibited a large steady state error relative to the uncalibrated controller was able to correct. Figure 13 shows the uncalibrated controller's transient learning phase and eventual convergence on Jacobian elements that are able to drive the microrobot to the target position. Because the proportional controller does not update its Jacobian elements, it was not able to overcome steady state error.

While it was promising that the uncalibrated controller worked through steady state error that the proportional controller could not account for, different traditional control methods such as proportional integral control could accomplish this feat. The true test of the uncalibrated control was whether the controller could adapt to a changing system structure that the classical controller could not handle. Three separate system alterations were tested to determine the nature of the uncalibrated control.

The first alteration to the system architecture involved increasing the zoom and decreasing the field of view for the top camera. The results are shown in Figure 14.

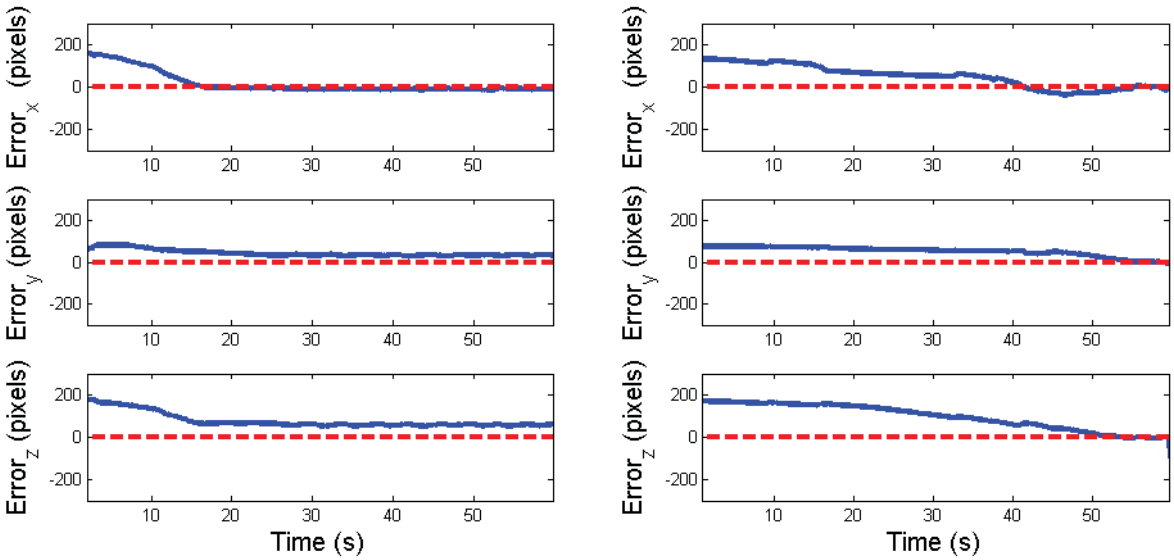

Figure 14. Error between the target and actual microrobot position with the top camera adjusted to a different zoom setting. The left graph shows the error of the proportional controller and the right graph shows the error of the uncalibrated controller.

The system's results for the increased zoom of the first camera were comparable to the system's results in the nominal state. The steady state error of the proportional controller remained close to approximately 30 pixels in the *y*-axis and 50 pixels in the *z*-axis in both cases. The uncalibrated controller was still able to overcome the steady state error, but Figure 15 shows that the method in which it did so was different between the two cases.

Because of the change in the system architecture, the values of the estimated Jacobian matrix converged to different values. This difference shows that the uncalibrated controller adapted to a changing environment in order to drive the microrobot to a target position.

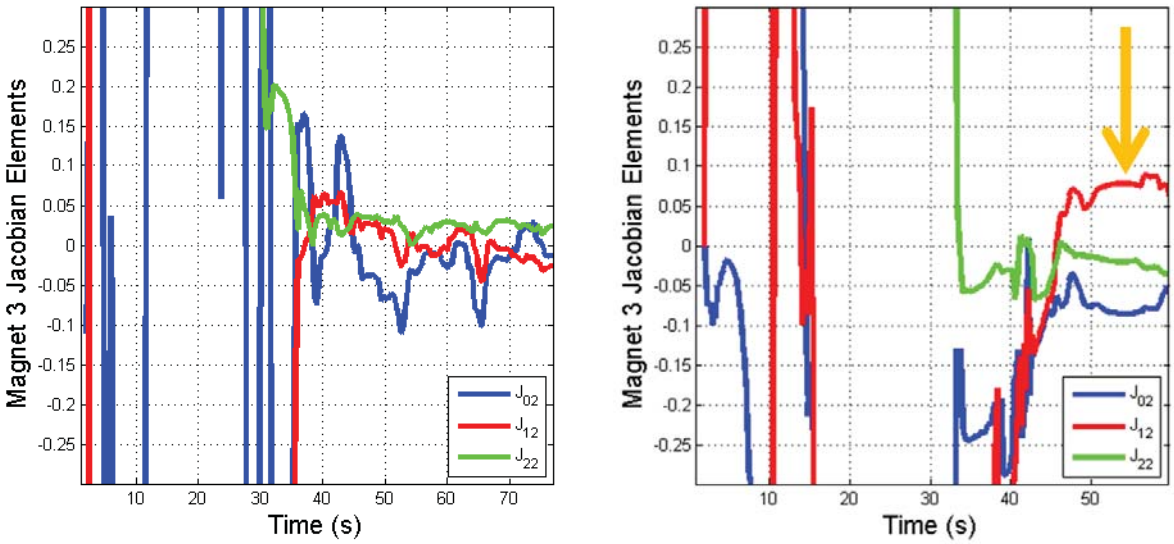

Figure 15. Jacobian values from the uncalibrated controller. The left graph shows values from the nominal state and the right graph shows values from when the top camera was adjusted to a different zoom. The orange arrow highlights that the magnitude of the Jacobian element increased.

The second alteration to the system architecture involved lowering the voltage supplied to one of the electromagnet pairs. Electromagnet pair 3 (which controls the *y*-axis) was supplied with 24 Volts instead of the nominal 25 Volts. The results are shown in Figure 16.

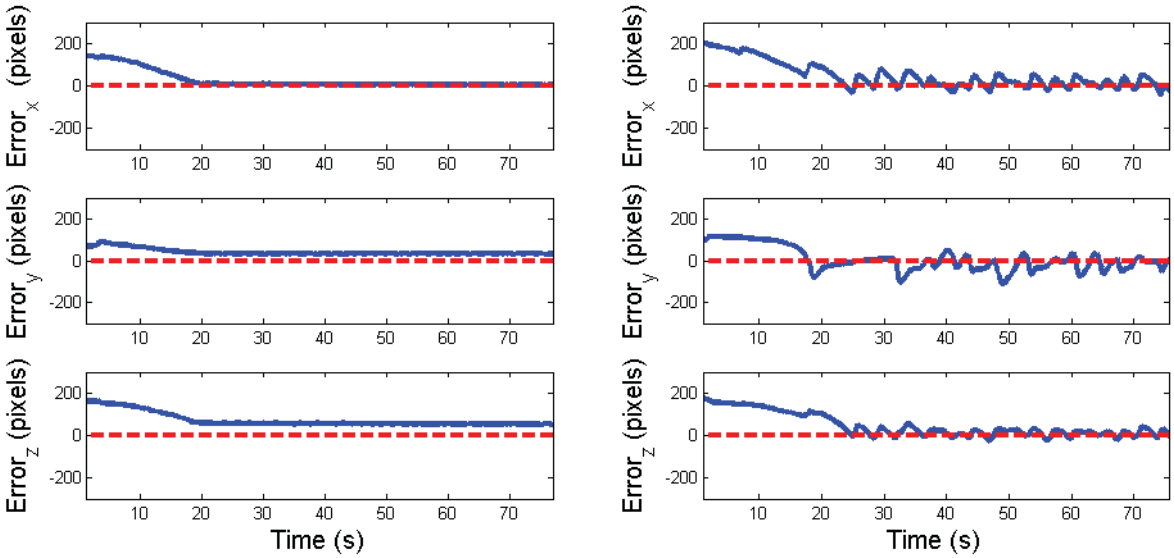

Figure 16. Error between the target and actual microrobot position with the voltage supplied to electromagnet pair 3 reduced to 24 Volts. The left graph shows the error of the proportional controller and the right graph shows the error of the uncalibrated controller.

With the reduction of the supplied voltage to electromagnet pair 3, the steady state in the proportional controller increased to approximately 35 pixels in the *y*-axis while the steady state in the *z*-axis remained at approximately 50 pixels. The lowered voltage also affected the uncalibrated controller's ability to keep the microrobot at the target location. Compared to the path of the uncalibrated controller in nominal state of the system, the uncalibrated controller with the reduced voltage struggled to maintain the target position against the pull of gravity, resulting in a bobbing behavior.

Again the change in the system architecture meant that the estimated Jacobian matrix converged to a different set of values. Figure 17 shows a distinct increase in the 2nd row and 2nd column value of the Jacobian, which relates control of the *y*-axis to the power sent to electromagnet pair three. This increase is logical because there is less voltage supplied to electromagnet pair three, so the estimator makes up for this by increasing the value of the Jacobian that relates to this degree of freedom.

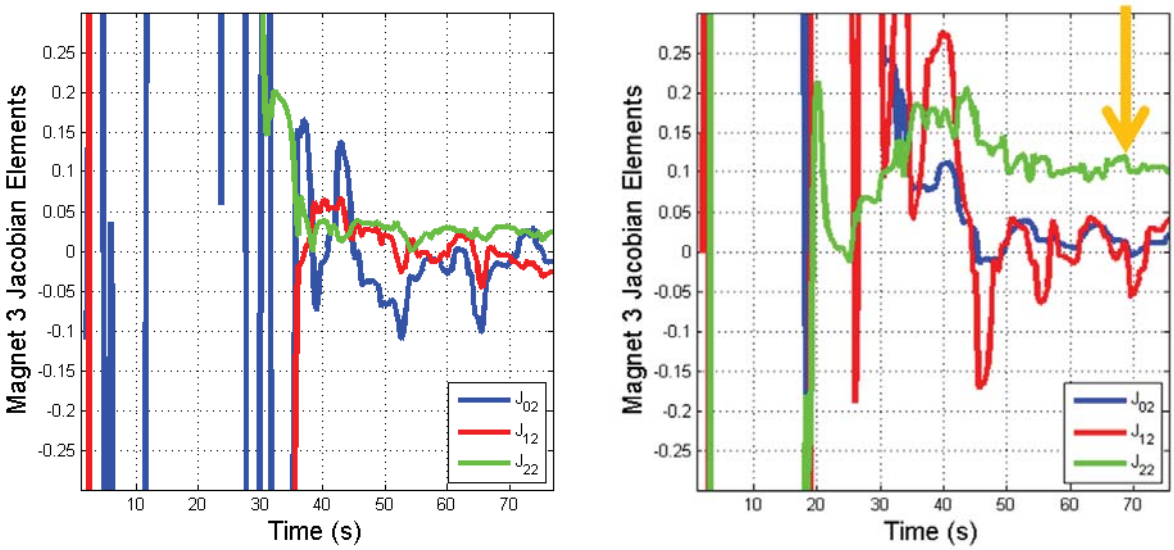

Figure 17. Jacobian values from the uncalibrated controller. The left graph shows values from the nominal state and the right graph shows values from when voltage supplied to electromagnet pair 3 was reduced to 24 Volts. The orange arrow highlights that the Jacobian element which relates to electromagnet pair 3 increased.

The third alteration to the system involved reversing the order of the electromagnet pairs. In the nominal state, a control signal of +50 would activate electromagnet 1B. In the adjusted state of the system, a control signal of +50 would activate electromagnet 1A instead. The results are shown in Figure 18 and 19.

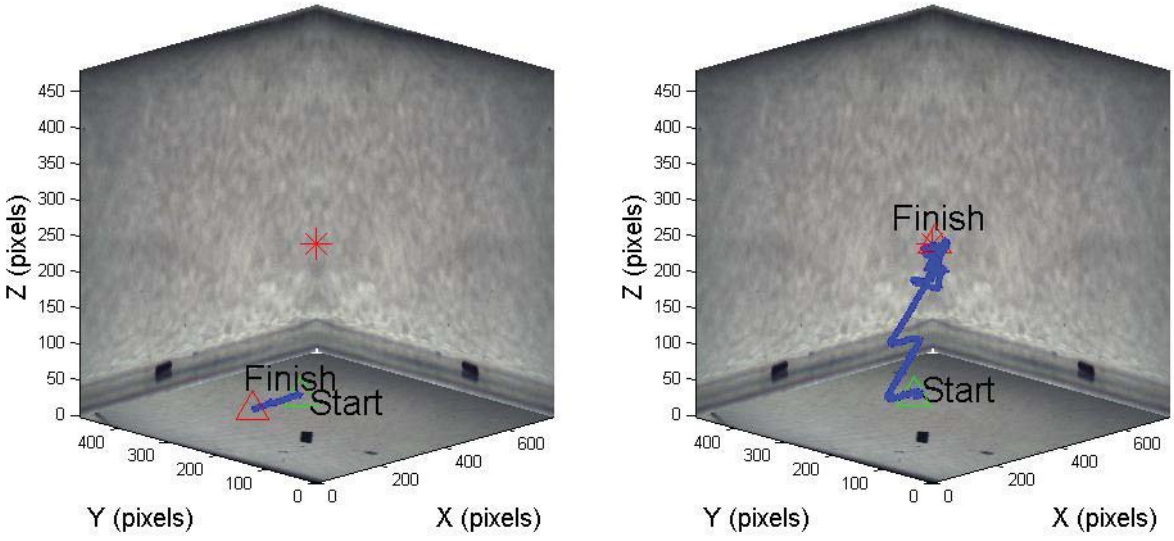

Figure 18. Three-dimensional path of the microrobot with the electromagnet pairs reversed. The left graph shows the path in the image space of the proportional controller and the right graph shows the path in the image space of the uncalibrated controller.

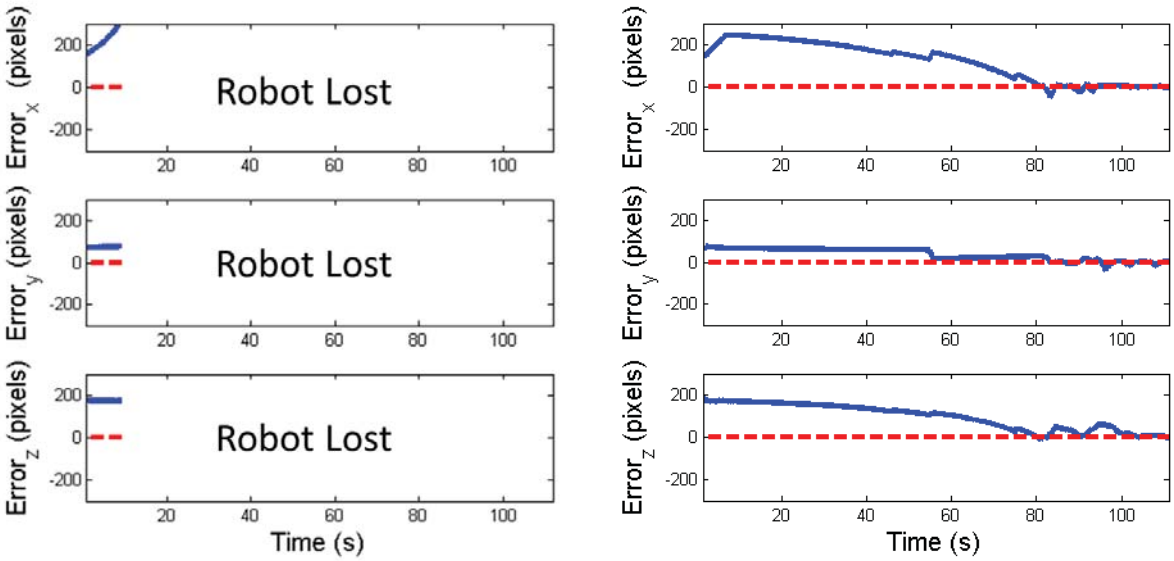

Figure 19. Error between the target and actual microrobot position with the electromagnet pairs reversed. The left graph shows the error of the proportional controller and the right graph shows the error of the uncalibrated controller.

Figure 18 and 19 show that the proportional controller was not able to handle the reversal of the electromagnet pairs which is a pathological change to the system's architecture. Within ten seconds, the proportional controller pulled the microrobot the wrong direction until it was outside the view of the camera vision system. Once the microrobot is lost by the camera system, error data and Jacobian values are no longer transmitted.

While settling time was increased, Figure 20 shows that the steady state values of the estimated Jacobian matrix for the altered system were again significantly different than the estimated values in the nominal system. The reversal of the electromagnet pairs caused the Jacobian matrix values to switch signs. The uncalibrated controller was able to overcome this significant change to the system's architecture and maintain the microrobot's position at the target position.

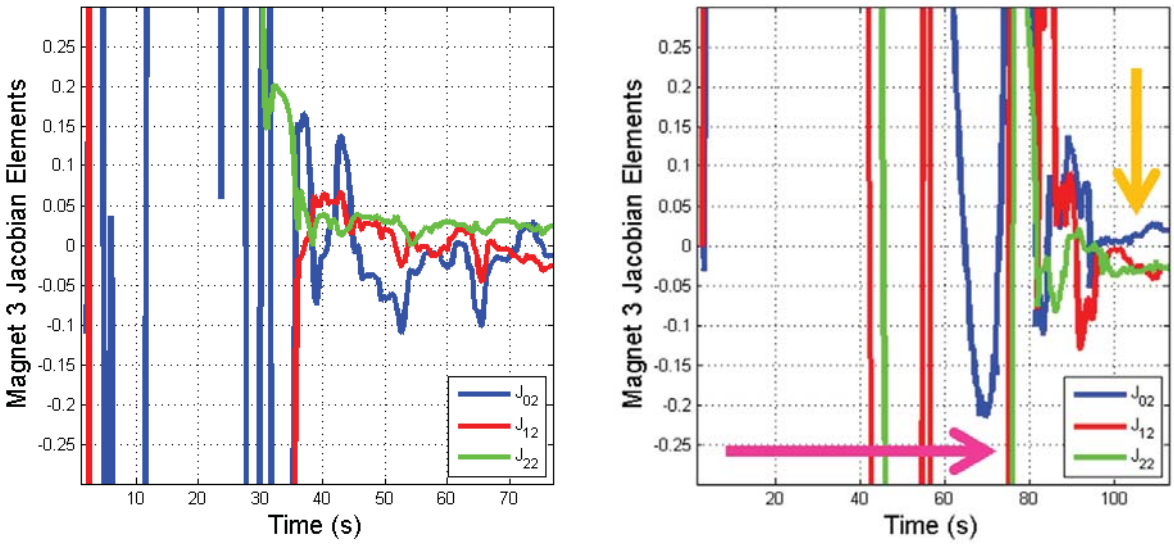

Figure 20. Jacobian values from the uncalibrated controller. The left graph shows values from the nominal state and the right graph shows values from when the electromagnet pairs were reversed. The orange arrow highlights that the Jacobian elements converged to values of opposite signs. The pink arrow highlights the increased time needed to achieve stability.

Figures 14 through 20 demonstrate the success of the uncalibrated control system for three significant system alterations: a change in the vision system, a change in the actuation system, and a change in the controller. In each of these cases, no changes were made to the initial conditions for the Jacobian estimation algorithm. In each case, convergence on the target position was achieved.

While the uncalibrated control system successfully overcame these three system alterations, reliability remains an issue at this time. Variability due to system noise and disturbances sometimes results in an initial actuation of an electromagnet pair that can pull the microrobot outside the vision system's view. Despite the issues with reliability, the achievement of three-dimensional, uncalibrated, vision based control is novel to the field of microrobotics.

V. DISCUSSION

A. Future Work

While the uncalibrated, three-dimensional microrobot control system met every designed goal, there are always improvements that can be made to make the system more robust. Changes to the design of the controller could both increase the reliability and expand the capabilities of the system. To make the controller more dependable, the fact that the buoyancy forces and the gravitational forces are not equivalent could be accounted for in the design of the uncalibrated controller. Similar changes to the control algorithm could be made to drive the robot towards moving targets or trajectories. Similarly, the controller could be modified to enable the manipulation of an object in the microrobot's workspace. This capability would further the emerging fields of microassembly and microsurgery.

Changes to the physical system could include improving the vision system by increasing the field of view of the cameras to encompass the entire operating arena or altering the electromagnet and camera orientation in order to better counteract the effects of gravitational forces. Also, the microrobot could be specifically designed to be closer to neutral buoyancy in a saline solution.

B. Summary of Accomplishments

The Naval Academy's two-dimensional microrobot control system was expanded to a three-dimensional microrobot control system. The two-dimensional vision capabilities were augmented with the addition of another camera to measure the position of the microrobot in the *z*-axis. The addition of two electromagnets with improved driver circuitry achieved three-dimensional actuation. A LabVIEW program was created that can utilize: an open-loop user controlled system; a proportional controller; and an uncalibrated controller. The uncalibrated controller implemented a novel, Recursive Least Square Jacobian estimation algorithm to regulate the position of a microrobot operating in a three-dimensional fluid volume. Through testing of the created system, the capability of the uncalibrated controller to adapt to system changes that thwarted the control efforts of the proportional controller was proven. The successful completion of the project's goals has is an important contribution to the field of microrobotics. While others have achieved three-dimensional microrobot control, this work is the first demonstration of uncalibrated control in three dimensions.

VI. BIBLIOGRAPHY

[1] J. A. Piepmeier, C. Olsen and S. L. Firebaugh, "Uncalibrated Trajectory Following with Magnetically Controlled Microrobots," *MEMS & NEMS (MAMNA), 2014 Spring Symposium: From Lab to Life: Field Based Applications of, IEEE,* pp. 1-6, 2014.

[2] J. A. Piepmeier, S. Firebaugh and C. S. Olsen, "Uncalibrated Visual Servo Control of Magnetically Actuated Microrobots in a Fluid Environment," *Micromachines,* vol. 5, no. 4, pp. 797-813, 2014.

[3] A. Ghanbari, P. H. Chang, H. Choi and B. J. Nelson, "Time Delay Estimation for Control of Microrobots under Uncertainties," in *IEEE/ASME International Conference on Advanced Intelligent Mechatronics (AIM)*, Wollongong, Australia, 2013.

[4] T. R. Kuphaldt, Lessons In Electric Circuits: Volume II - AC, ReadCycle, 2011.

[5] K. B. Yesin, K. Vollmers and B. J. Nelson, "Analysis and Design of Wireless Magnetically Guided Microrobots in Body Fluids," in *International Conference on Robotics & Automation*, New Orleans, LA, April 2004.

[6] K. Hosoda and M. Asada, "Versatile visual servoing without knowledge of true jacobian," in *IEEE/RSJ International Conference on Intelligent Robots and Systems (IROS)*, 1994.

[7] M. Jagersand, O. Fuentes and R. Nelson, "Experimental evaluation of uncalibrated visual servoing for precision manipulation," in *IEEE Int. Conf. on Robotics and Automation*, 1997.

[8] J. A. Piepmeier, G. V. McMurray and H. Lipkin, "Uncalibrated dynamic visual servoing," *IEEE Trans. on Robotics and Automation,* vol. 20, pp. 143-147, 2004.

[9] J. A. Piepmeier, A dynamic quasi-newton method for model independent visual servoing, Atlanta, GA USA: Georgia Institute of Technology, 1999.

[10] E. Eleftheriou and D. D. Falconer, "Tracking properties and steady-state performance of rls adaptive filter algorithms," *Acoustics, Speech and Signal Processing, IEEE Transactions on,* vol. 34, pp. 1097-1110, 1986.

[11] Magnetech Corporation, "DC Opposite Pole Electromagnets," Electromagnets purchased: OP 1212, OP 2025, OP 3030, 18 November 2014. [Online]. Available: http://www.magnetechcorp.com/opposite_pole.html. [Accessed 07 December 2014].

[12] W. Jing and D. Cappelleri, "A Magnetic Microrobot with in situ Force Sensing Capabilities," *Robotics: MDPI,* vol. 3, pp. 106-119, 2014.